Genetic and pharmacologic inhibition of EPHA2 promotes apoptosis in NSCLC

Katherine R. Amato,[1] Shan Wang,[2] Andrew K. Hastings,[3] Victoria M. Youngblood,[1] Pranav R. Santapuram,[1] Haiying Chen,[4] Justin M. Cates,[3,5] Daniel C. Colvin,[6] Fei Ye,[7] Dana M. Brantley-Sieders,[2,5] Rebecca S. Cook,[1,5] Li Tan,[8,9] Nathanael S. Gray,[8,9] and Jin Chen[1,2,5,10,11]

[1]Department of Cancer Biology, [2]Division of Rheumatology and Immunology, and [3]Department of Pathology, Microbiology, and Immunology, Vanderbilt University, Nashville, Tennessee, USA. [4]The University of Melbourne, Melbourne, Victoria, Australia. [5]Vanderbilt-Ingram Cancer Center, Vanderbilt University, Nashville, Tennessee, USA. [6]Vanderbilt University Institute of Imaging Science and [7]Department of Biostatistics, Vanderbilt University, Nashville, Tennessee, USA. [8]Department of Biological Chemistry and Molecular Pharmacology, Harvard Medical School, Boston, Massachusetts, USA. [9]Dana-Farber Cancer Institute, Harvard Medical School, Boston, Massachusetts, USA. [10]Department of Cell and Developmental Biology, Vanderbilt University, Nashville, Tennessee, USA. [11]Veterans Affairs Medical Center, Tennessee Valley Healthcare System, Nashville, Tennessee, USA.

Genome-wide analyses determined previously that the receptor tyrosine kinase (RTK) EPHA2 is commonly overexpressed in non–small cell lung cancers (NSCLCs). EPHA2 overexpression is associated with poor clinical outcomes; therefore, EPHA2 may represent a promising therapeutic target for patients with NSCLC. In support of this hypothesis, here we have shown that targeted disruption of *EphA2* in a murine model of aggressive *Kras*-mutant NSCLC impairs tumor growth. Knockdown of *EPHA2* in human NSCLC cell lines reduced cell growth and viability, confirming the epithelial cell autonomous requirements for EPHA2 in NSCLCs. Targeting *EPHA2* in NSCLCs decreased S6K1-mediated phosphorylation of cell death agonist BAD and induced apoptosis. Induction of *EPHA2* knockdown within established NSCLC tumors in a subcutaneous murine model reduced tumor volume and induced tumor cell death. Furthermore, an ATP-competitive EPHA2 RTK inhibitor, ALW-II-41-27, reduced the number of viable NSCLC cells in a time-dependent and dose-dependent manner in vitro and induced tumor regression in human NSCLC xenografts in vivo. Collectively, these data demonstrate a role for EPHA2 in the maintenance and progression of NSCLCs and provide evidence that ALW-II-41-27 effectively inhibits EPHA2-mediated tumor growth in preclinical models of NSCLC.

Introduction

Genome-wide expression analyses of human lung cancer have identified a number of receptor tyrosine kinases (RTKs) as overexpressed and potentially representing drivers of non–small cell lung cancer (NSCLC) (1–4). Among these RTKs was EPHA2, which belongs to the largest family of RTKs, the EPH family. EPH family proteins have been recognized increasingly as key regulators of both normal development and disease (reviewed in refs. 5–7). EPH molecules contain a single transmembrane-spanning domain and distinct domains for ligand binding, receptor clustering, and signaling. Binding of EPH receptors to their ligands, known as EPHRINS, induces receptor clustering and activation. In addition to ligand-induced receptor activities, EPH receptors can also be activated by other cell-surface receptors, such as EGFR and ERBB2 (8, 9). Multiple intracellular signaling pathways have been linked to EPH receptors, including RAS/RAF/MAPK, PI3K/AKT/mTOR, SRC, FAK, ABL, and RHO/RAC/CDC42 (reviewed in refs. 5–7). An oncogenic role for EPHA2 has been suggested due to its overexpression in lung cancer as well as the correlation of high levels of EPHA2 with smoking, brain metastasis, disease relapse, and overall poor patient survival (10–12). However, the biological and clinical relevance underlying these observations remains poorly understood.

Similar to what is seen in lung cancers, EPHA2 is overexpressed in a number of other cancers, including breast cancer. Preclinical models provide compelling evidence that EPHA2 overexpression increases breast tumor formation, malignant progression, and therapeutic resistance to antitumor therapies (9, 13). Large-scale expression profiling for *EPHA2* transcript levels in relation to clinical outcome revealed a negative association between *EPHA2* transcript levels and overall survival in breast cancer (14). These findings are consistent with preclinical studies in genetically engineered mouse models of breast cancer, which revealed distinct roles for EPHA2 in the tumor epithelia, in which EPHA2 signaling drives tumor cell proliferation and survival, and in the tumor microenvironment, in which EPHA2 is required for tumor angiogenesis (9, 15, 16). Thus, therapeutic inhibition of EPHA2 in breast cancers may provide a dual benefit to the patient, targeting both the tumor cells and the tumor microenvironment. The role of EPHA2 in lung tumor growth and/or angiogenesis is not yet clear.

In this study, we used a genetically engineered mouse model of NSCLC driven by mutant *Kras* to demonstrate that gene targeting of *EphA2* decreased growth and progression of spontaneous NSCLCs. We found that RNAi-mediated silencing of *EPHA2* inhibited the number of viable tumor cells in a panel of human NSCLC cell lines in vitro. Targeting *EPHA2* in KRAS mutant NSCLCs decreased S6K1-mediated BAD phosphorylation and induced apoptosis. Using human NSCLC xenografts, we found that inducible loss of *EPHA2* from preexisting tumor cells decreased tumor growth. Furthermore, an ATP-competitive, small-molecule tyrosine kinase inhibitor for EPHA2 decreased tumor cell viability in vitro and tumor growth in vivo. Collectively, these studies identify EPHA2 as a promising therapeutic target for NSCLCs.

Conflict of interest: The authors have declared that no conflict of interest exists.
Citation for this article: *J Clin Invest.* 2014;124(5):2037–2049. doi:10.1172/JCI72522.

Results

EPHA2 promotes tumor growth in a transgenic mouse model of spontaneous NSCLC. Under physiological conditions, *EphA2*-deficient mice produced by gene targeting are viable, fertile, and healthy. However, previous studies demonstrated that *EphA2* loss decreases growth of transgenic mouse mammary tumors and decreases tumor angiogenesis (9, 16). We therefore used the *EphA2*-deficient mouse model to determine whether EPHA2 is required in a transgenic mouse model of NSCLC, encoding a latent $Kras^{G12D}$ allele knocked in at the endogenous *Kras* locus (17). In this model, lung cancers driven by the active mutant $Kras^{G12D}$ develop spontaneously within the innate tissue microenvironment, recapitulating human lung cancer pathology. To assess tumor burden in $Kras^{G12D}EphA2^{+/+}$ and $Kras^{G12D}EphA2^{-/-}$ mice, we measured total lung wet weight over a time course. We found that $Kras^{G12D}$ tumor-bearing lungs were heavier than tumor-free lungs lacking $Kras^{G12D}$ expression (Figure 1A), suggesting that lung weight correlates with tumor burden. A reduction in lung wet weight was observed in $Kras^{G12D}EphA2^{-/-}$ mice compared with that in $Kras^{G12D}EphA2^{+/+}$ controls. Importantly, tumor-free lungs harvested from $EphA2^{-/-}$ mice were similar in weight to those harvested from tumor-free $EphA2^{+/+}$ mice, indicating that the decreased lung weight seen in $Kras^{G12D}EphA2^{-/-}$ mice was due to reduced tumor burden. It is possible, however, that lung weight could be altered as a result of changes in interstitial fluid volume in the lung because of the known role of EPHA2 in angiogenesis. To distinguish between these possibilities, tumor burden was assessed by two additional methods. First, we measured the area of tumors on the surface of lungs harvested at 3 time points (Figure 1B), demonstrating a decreased burden of surface lung tumors in $Kras^{G12D}EphA2^{-/-}$ mice compared with that in $Kras^{G12D}EphA2^{+/+}$ mice. Additionally, lung cancer progression in $Kras^{G12D}EphA2^{+/+}$ and $Kras^{G12D}EphA2^{-/-}$ mice was monitored using MRI, beginning at 15 weeks of age, when tumors were evident in both groups of mice (Figure 1C). $Kras^{G12D}EphA2^{-/-}$ lung tumors were smaller than tumors in $Kras^{G12D}EphA2^{+/+}$ mice at 15 weeks of age, and this difference became more pronounced at 20 and 25 weeks of age (Figure 1D).

Histological analysis of the lungs demonstrated the presence of tumors in both $Kras^{G12D}EphA2^{+/+}$ and $Kras^{G12D}EphA2^{-/-}$ mice and the absence of EPHA2 expression in *EphA2*-knockout mice (Figure 2, A and B, and Supplemental Figure 1A; supplemental material available online with this article; doi:10.1172/JCI72522DS1). Tumors were less frequent and smaller in size in $Kras^{G12D}EphA2^{-/-}$ mice compared with those in $Kras^{G12D}EphA2^{+/+}$ mice. Tumor cell apoptosis, as measured by TUNEL staining, was significantly higher in $Kras^{G12D}EphA2^{-/-}$ tumors compared with that in $Kras^{G12D}EphA2^{+/+}$ tumors (Figure 2, C and D), whereas tumor cell proliferation, as measured by PCNA immunohistochemistry, was unchanged in $Kras^{G12D}EphA2^{-/-}$ tumors (Figure 2, E and F). Because EPHA2 is known to promote tumor angiogenesis in breast cancer models (16), we assessed tumor microvessels in situ using immunofluorescence detection of vWF to visualize endothelial cells. These studies revealed a modest decrease in vWF-positive tumor vessels in $Kras^{G12D}EphA2^{-/-}$ tumors compared with that in $Kras^{G12D}EphA2^{+/+}$ tumors (Figure 2, G and H). Collectively, these results show that EPHA2 promotes progression of NSCLCs within their native microenvironment, such that genetic ablation of *EphA2* limited progression of this aggressive NSCLC tumor model.

Epithelial EPHA2 is required to maintain viable NSCLC cells. EPHA2 is overexpressed across all major histological subtypes of human NSCLC, and this overexpression is associated with poor clinical outcomes (10–12). Using a lentiviral-based shRNA strategy to silence *EPHA2* expression in a panel of 14 human NSCLC cell lines (Supplemental Table 1), we assessed the number of viable cells in culture 3 days after plating in media supplemented with 10% serum (Figure 3A). In 8 of 14 cell lines tested, *EphA2* shRNA (sh*EphA2*) reduced the number of viable tumor cells by more than 25% compared with cells treated with control shRNA (sh*Control*). Of these 8 NSCLC cell lines, 6 harbored activating *KRAS* mutations, 1 harbored an activating *NRAS* mutation, and 1 harbored an oncogenic *EGFR* mutation, highlighting EPHA2 as a potential therapeutic target across several NSCLC genetic subtypes, even the difficult-to-treat *KRAS* subtype. Western blot analysis performed in parallel with the MTT assays showed a substantial loss of EPHA2 protein expression in sh*EPHA2*-infected cells (Figure 3B). By 5 days after plating, sh*EPHA2*-infected cells that showed initial sensitivity to *EPHA2* inhibition demonstrated a further reduction in the number of viable tumor cells, with decreases ranging from 50% to 80% compared with that in sh*Control*-infected cells (Figure 3C, top 6 graphs). Cell lines most sensitive to *EPHA2* inhibition demonstrated higher EPHA2 receptor phosphorylation upon stimulation with either EPHRIN-A1 or serum (Supplemental Figure 1, B and C), suggesting that EPHA2 receptor activity drives an increase in viable NSCLC cells. While these data do not rule out the contribution of EPHA2 in the NSCLC microenvironment, this observation supports the hypothesis that targeting EPHA2 may be a feasible therapeutic approach for NSCLCs with heightened EPHA2 phosphorylation.

EPHA2 increases NSCLC tumor cell survival. To determine whether EPHA2 is required for NSCLC cellular survival, we assessed apoptosis in cells transfected with *EPHA2* siRNA (si*EPHA2*) sequences compared to that in those transfected with scrambled siRNA sequences. At 3 days after transfection, EPHA2 expression was reduced in the 6 cell lines transfected with si*EPHA2* as compared with that in those transfected with a scrambled siRNA sequence (Figure 4D and data not shown). Increased frequency of tumor cell death was observed in all 6 NSCLC cell lines transfected with si*EPHA2*, as measured by TUNEL analysis (Figure 4A) and cleavage of caspase-3 and PARP (Figure 4B). These results were confirmed using a cell death ELISA to detect histone-associated DNA fragmentation (Figure 4C), again revealing that si*EPHA2* increased apoptosis in each of the 6 cell lines. At the same time point, we collected cell lysates from serum-starved H2009 and H358, 2 cell lines with high EPHA2 receptor phosphorylation levels. Signaling studies in these cells revealed decreased basal phosphorylation levels of S6 kinase and its substrate ribosomal protein S6 (Figure 4D), while many pathways, including AKT and ERK, were not significantly affected by EPHA2 loss in the absence of serum. EPHA2-deficient cells stimulated for 10 minutes with 10% serum showed no alteration in the phosphorylation of ERK. However, serum-induced phosphorylation of p90-RSK, and AKT at a lesser extent, was reduced in si*EPHA2* cells, suggesting that EPHA2 is required to stimulate acute growth factor signaling from p90-RSK to S6 kinase and S6. Phosphorylation of the proapoptotic BH3-only protein BAD, which results in BAD inhibition and tumor cell survival, is another target of the p90-RSK/S6 kinase signaling pathway (18, 19). Interestingly, loss of *EPHA2* in si*EPHA2*-transfected cells caused a decreased level of BAD phosphorylation in serum-stimulated conditions, consistent with the increased levels of cell death seen in si*EPHA2*-transfected cells. Together, these data indi-

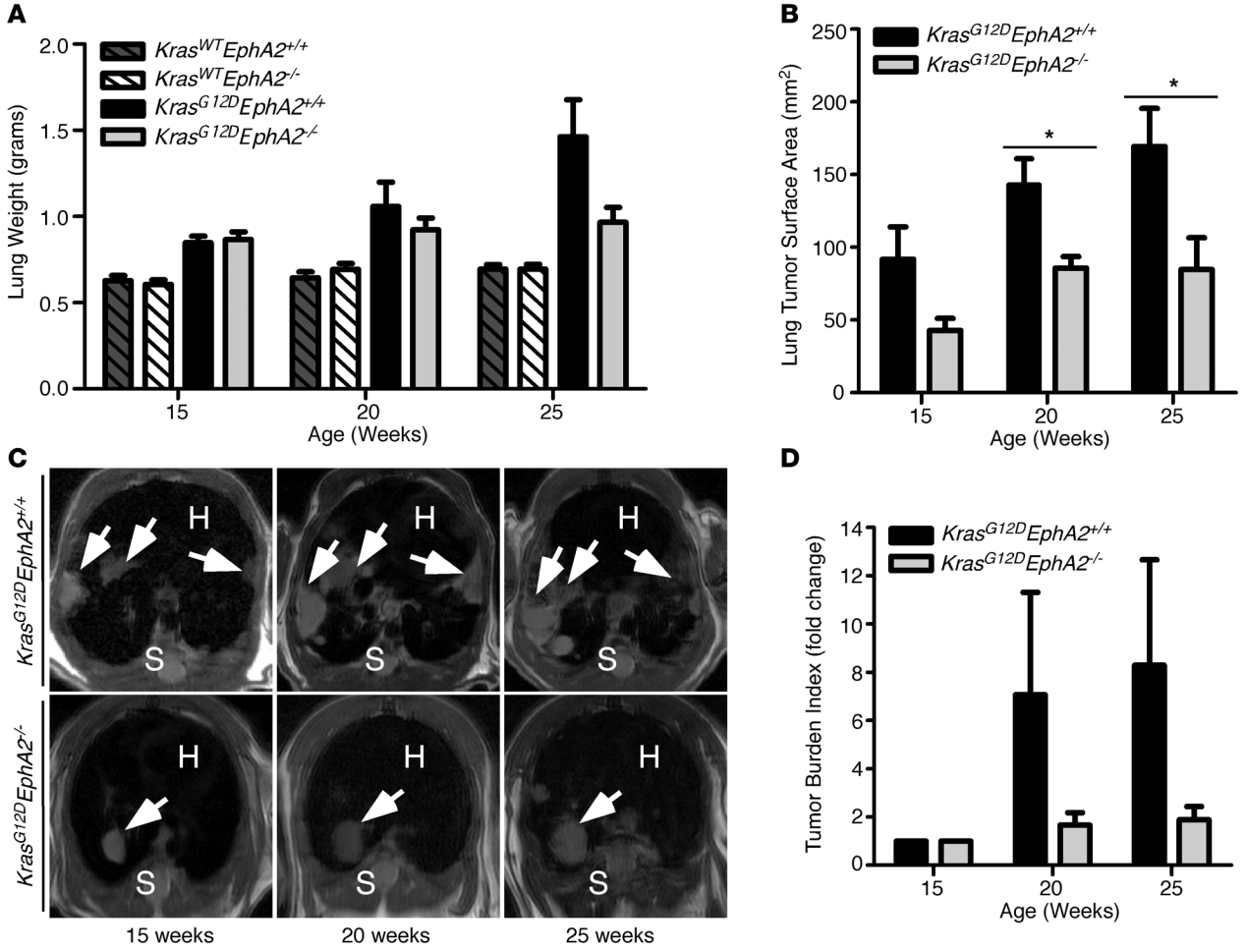

Figure 1

Loss of *EphA2* results in decreased tumor burden in a *Kras*^{G12D} knockin mouse model of spontaneous NSCLC. (**A**) Lungs of wild-type and *EphA2*-deficient mice were collected, and the total lung weight was measured at 15, 20, and 25 weeks of age to assess the additional mass contributed to the lungs by the tumor burden. Average lung weight ± SEM is shown (n = 10 per genotype). (**B**) Tumor area on the lung surface was measured by a digital caliper and presented as average lung tumor surface area ± SEM (n = 8 per genotype). (**C**) Wild-type and *EphA2*-deficient *Kras*^{G12D} mice were subjected to MRI at 15, 20, 25 weeks of age. T2-weighted MRI images were taken in the axial plane with slice thickness of 1 mm. Representative images at 15, 20, and 25 weeks are shown. White arrows indicate tumor tissue. H, heart; S, spine. (**D**) Tumor volumes were quantified as a composite of 10 serial MRI slices of the lung per mouse using Matlab software and were graphed as a tumor burden index relative to 15 weeks ± SEM (n = 5 per genotype). *P < 0.05.

cate that EPHA2 signaling is required within the tumor epithelial compartment of NSCLCs to maintain tumor cell survival.

EPHA2 knockdown in the tumor epithelial compartment decreases NSCLC growth in vivo. To assess the therapeutic potential of targeting EPHA2 in the context of preexisting NSCLC tumors, we transduced H358 cells with a lentivirus encoding doxycycline-inducible (DOX-inducible) shRNA sequences against *EPHA2* or a scrambled control sequence. DOX treatment of H358-sh*EPHA2* cells in culture resulted in decreased EPHA2 protein expression compared with that in untreated H358-sh*EPHA2* cells and DOX-treated H358-sh*SCRAMBLED* cells (Figure 5A). Similar to what was seen with stable shRNA-mediated *EPHA2* knockdown, DOX-induced knockdown of *EPHA2* decreased the number of viable cells by 70% of the number seen in untreated H358-sh*EPHA2* cells or DOX-treated H358-sh*SCRAMBLED* controls after 9 days in culture (Figure 5B). H358-sh*EPHA2* and H358-sh*SCRAMBLED* cells were injected into the left and right flanks of each mouse, respectively, to generate matched pairs of subcutaneous tumor xenografts. Once the tumor volume reached 200 mm^3, DOX was delivered in the mouse chow ad libitum. DOX-treated H358-sh*EPHA2* tumor growth was significantly inhibited compared with what was seen in DOX-treated H358-sh*SCRAMBLED* xenografts (Figure 5C), resulting in a 30% decrease in tumor volume after 35 days of DOX treatment (P < 0.0001). Western blot analysis using tumor lysates derived at the end of the study revealed a persistent decrease of EPHA2 protein levels in DOX -treated tumors (Figure 5D). Similar to previous data, a significant increase of apoptosis was observed in DOX-treated H358-sh*EPHA2* cells compared with that in untreated H358-sh*EPHA2* cells and DOX-treated H358-sh*SCRAMBLED* cells (Figure 5, E and F). PCNA immunohistochemical analysis of tumor sections indicated no change in the proliferation of H358-sh*EPHA2* cells relative to H358-sh*SCRAMBLED* cells (Figure 5, G and H). No statistically sig-

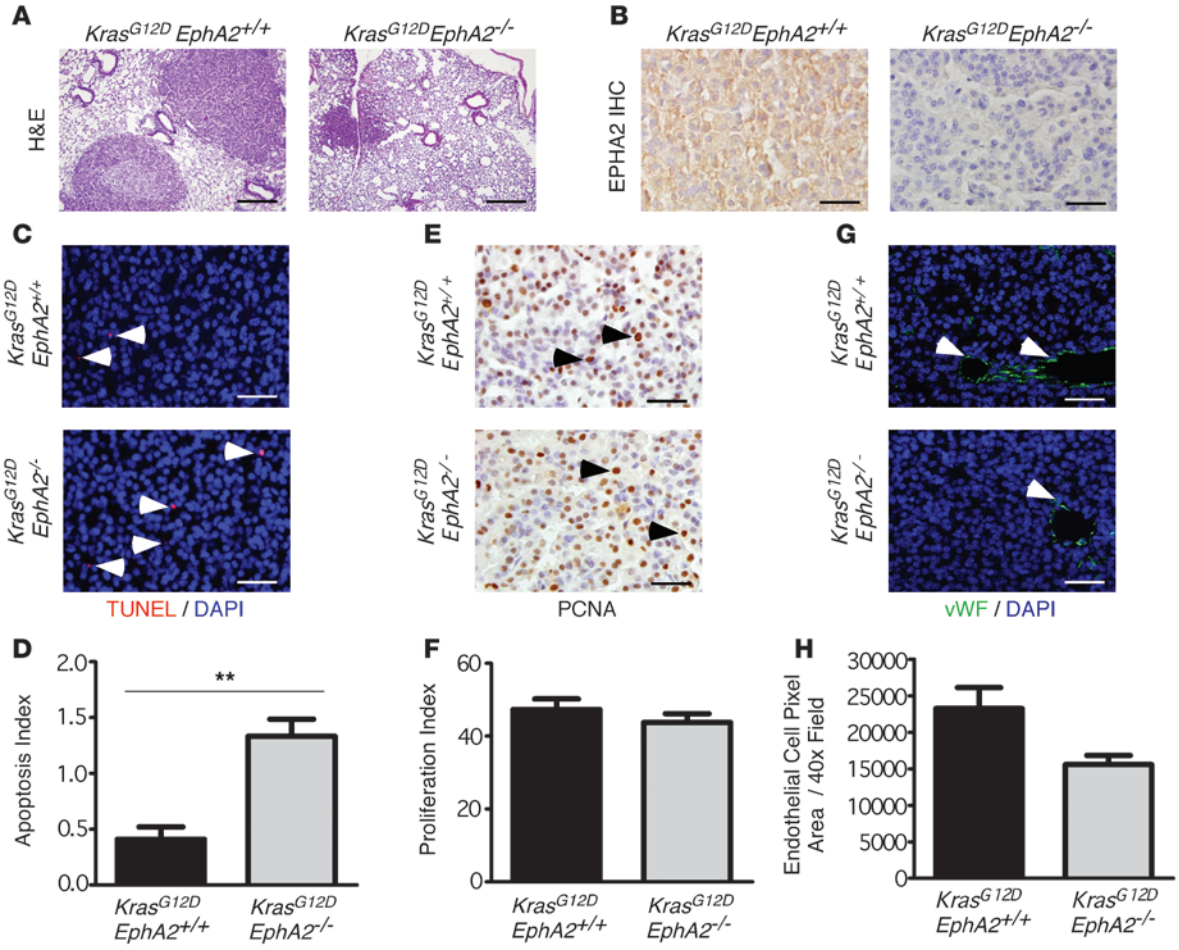

Figure 2

EphA2 deficiency results in increased apoptosis in *Kras*^{G12D} tumors. (**A**) H&E-stained lung sections (25 weeks) showing tumors derived from *Kras*^{G12D}*EphA2*$^{-/-}$ mice relative to those derived from *Kras*^{G12D}*EphA2*$^{+/+}$ mice. Scale bar: 200 μm. (**B**) Loss of EPHA2 protein expression in tumors was confirmed by immunohistochemistry (IHC). Scale bar: 50 μm. (**C**) Apoptosis in tumor sections was measured by the TUNEL assay. TUNEL^{+} nuclei (red) are indicated with arrowheads. Scale bar: 50 μm. (**D**) Apoptosis was quantified as a percentage of TUNEL-positive nuclei relative to the total nuclei. Apoptosis index is presented as average percentage of TUNEL-positive nuclei per total nuclei ± SEM (n = 6 per genotype). (**E**) Tumor cell proliferation was assessed by PCNA immunohistochemistry. Arrowheads indicate representative proliferating nuclei. Scale bar: 50 μm. (**F**) Proliferation was quantified by assessing the total number of PCNA^{+} nuclei (brown) compared with the total nuclei. Proliferation index is presented as average percentage of PCNA-positive nuclei per total nuclei ± SEM (n = 6 per genotype). (**G**) Tumor vasculature was assessed by vWF immunofluorescence (green). Arrowheads indicate tumor microvessels. Scale bar: 50 μm. (**H**) Microvessels in the tumor were quantified by measuring vWF^{+} pixels in each tumor field ± SEM (P = 0.07) (n = 6 per genotype). **P < 0.01.

nificant change was observed in tumor blood vessels in any of the treatment conditions (Figure 5, I and J). These results demonstrate that inhibition of EPHA2 within the established tumor epithelium is capable of decreasing growth of NSCLCs in vivo.

An EPHA2 kinase inhibitor suppresses growth of NSCLC in vitro and in vivo. We tested more than 50 small molecules predicted to inhibit EPHA2 tyrosine kinase activity, revealing that the compound ALW-II-41-27 had the most potent effect on tumor cell viability (data not shown). ALW-II-41-27 is a type II small-molecule inhibitor that targets the ATP-binding pocket of the kinase domain as well as an allosteric site next to the "DFG" motif in the receptor (refs. 20, 21, and Figure 6A). A compound with similar structure, NG-25 (22), was used as a control, because it possessed a very similar profile of kinase targets as that of ALW-II-41-27, with EPHA2 being a notable exception. ALW-II-41-27 inhibits EPHA2 with an enzymatic IC_{50} of 11 nM compared with an IC_{50} of 770 nM for NG-25, as measured by an in vitro kinase assay (Supplemental Table 2). In lung cancer cells, 1 μM ALW-II-41-27 impaired tyrosine phosphorylation of the EPHA2 receptor in H358 cells within 15 minutes and continued to inhibit EPHA2 tyrosine phosphorylation through 6 hours of treatment (Figure 6B). In contrast, NG-25 showed no effect on EPHA2 phosphorylation at the same concentration. ALW-II-41-27 also inhibited ligand-induced EPHA2 phosphorylation in a dose-dependent manner (Figure 6C). Furthermore, depletion of *EPHA2* by RNAi rendered NSCLC cell lines much less sensitive to the effects of ALW-II-41-27 relative to undepleted controls, consistent with EPHA2 being a functionally important target of the compound (Figure 6, D and E).

Next, we assessed cell viability in NSCLC cells treated with ALW-II-41-27. H358 cells treated over a 72-hour time course with 1 μM

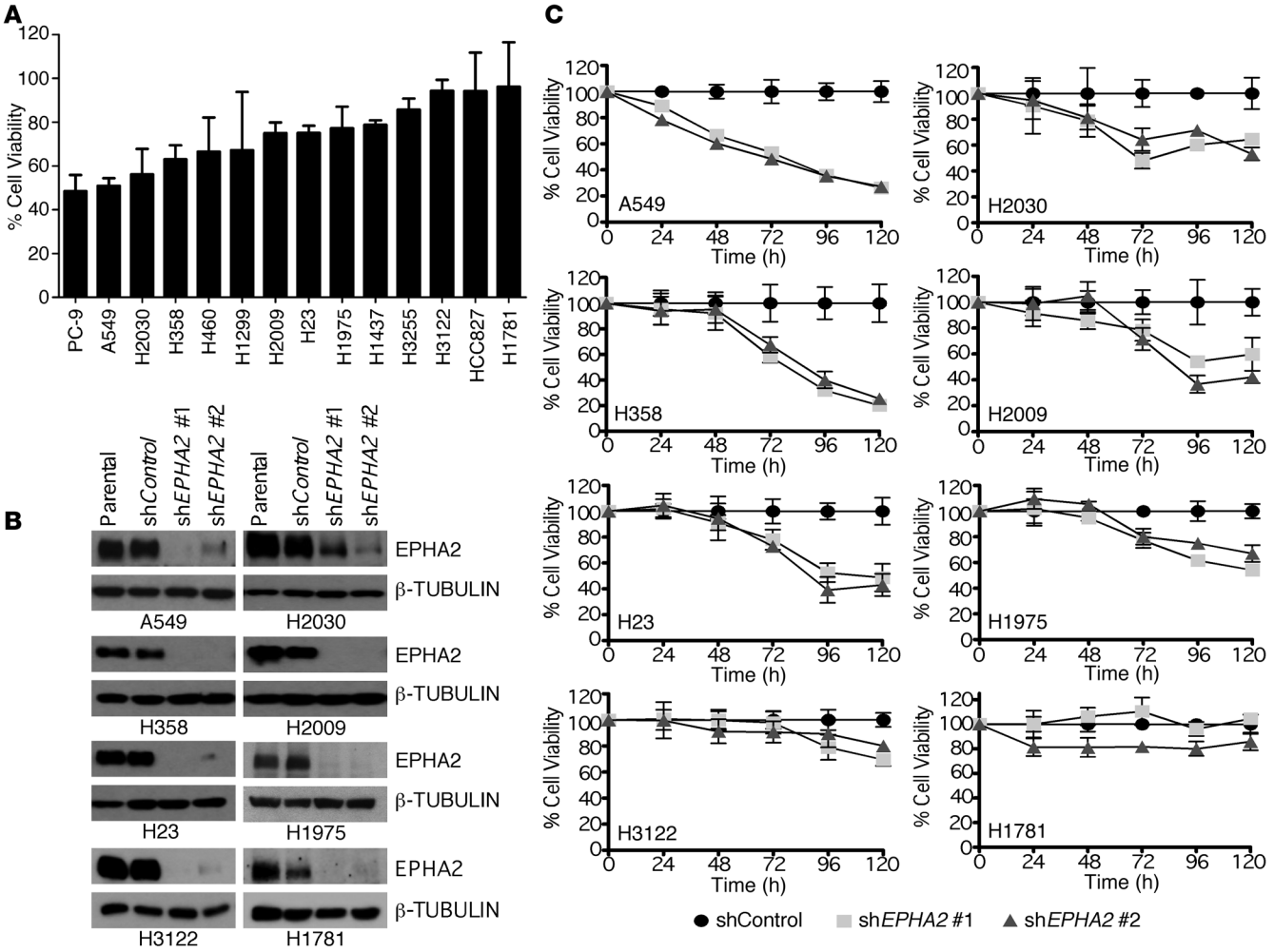

Figure 3

Effects of knockdown of *EPHA2* on a panel of NSCLC cell lines. (**A**) 14 NSCLC cell lines were transduced with lentiviruses containing either sh*EPHA2* or a pLKO.1 vector control. The resulting cell populations were selected in 1 to 2 μg/ml puromycin for 5 days. Cell viability was analyzed by the MTT assay at 72 hours after puromycin selection. Experiments were repeated twice with 6 replicates per experiment. Data were pooled and are presented as viability of sh*EPHA2* knockdown cells relative to that of the vector control cells ± SEM. (**B**) Immunoblotting for EPHA2 expression confirmed knockdown in 8 NSCLC cell lines. β-Tubulin expression was used as a loading control. (**C**) Cells were treated as in **A**, and cell viability was assessed over 5 days. Experiments were repeated twice, and data were pooled and are presented as shRNA knockdown relative to the vector control cells ± SEM.

ALW-II-41-27 displayed a time-dependent decrease in the number of viable tumor cells compared with cells treated with 1 μM NG-25 (Supplemental Figure 2A). Five additional NSCLC lines were also tested, and a 40%–80% reduction in the number of viable tumor cells after 72 hours in the presence of 1 μM ALW-II-41-27 as compared with treatment with 1 μM NG-25 was observed (Figure 7A, top 6 graphs). Two cell lines (H3122 and H1781) that were resistant to EPHA2 knockdown were also less sensitive to ALW-II-41-27. Cell death was increased in response to ALW-II-41-27 in H358 cells (Supplemental Figure 2B), suggesting that pharmacologic EPHA2 inhibitors reproduce the effects obtained using genetic methods of EPHA2 inhibition and may be therapeutically advantageous in the treatment of NSCLC. To assess the intracellular consequences of targeting EPHA2 by ALW-II-41-27, cell lysates were collected from serum-starved H2009 and H358 cells treated with ALW-II-41-27 or DMSO for 6 hours. Western signaling analysis revealed decreases in both the basal and serum-stimulated phosphorylation of S6K1, S6, and BAD (Figure 7B), which is similar to the results seen in *EPHA2* knockdown experiments. These data suggest that ALW-II-41-27 inhibits EPHA2 signaling pathways necessary to maintain cell survival in NSCLC.

To assess the efficacy of the EPHA2 inhibitor in vivo, we treated 200 mm^3 H358 xenograft tumors with ALW-II-41-27, NG-25, or the vehicle alone. Initial pharmacokinetic analysis of ALW-II-41-27 following intravenous (1 mg/kg) and oral administration (10 mg/kg) revealed a relatively short half-life ($t_{1/2}$ = 0.83 hour), low plasma exposure (AUC = 333.7 nM/l), and low oral bioavailability (bioavailability = 24.6%). To compensate for this poor pharmacokinetic profile, mice were treated twice daily with 15 mg/kg ALW-II-41-27 via intraperitoneal injection. Administration of ALW-II-41-27 to tumor-bearing animals for 14 days significantly inhibited tumor growth of H358 tumors (Figure 8A). Toxicity

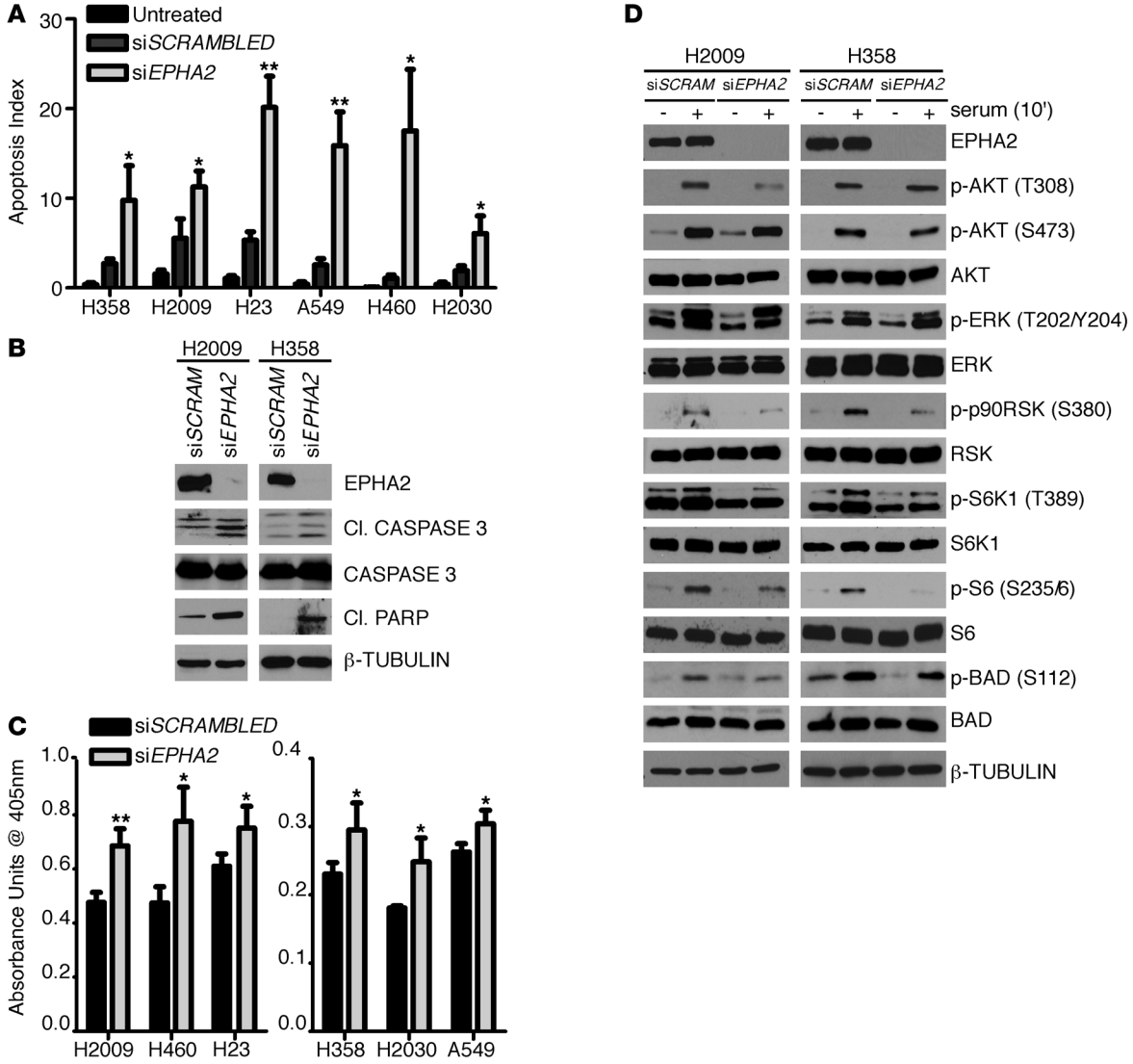

Figure 4

EPHA2 knockdown leads to an increase in apoptosis in NSCLC cell lines. (**A**) Cells were treated with scrambled or *EPHA2*-specific siRNA for 72 hours. Apoptosis was detected via the ApopTag TUNEL assay. Graph represents 3 independent experiments, and data are presented as the percentage of TUNEL-positive nuclei of total nuclei ± SEM. (**B**) Western blotting of H2009 and H358 cells treated with scrambled or si*EPHA2* for 72 hours with 5 μg/ml TRAIL added during the final 24 hours after transfection. Cl., cleaved (caspase-3 or PARP). (**C**) Apoptosis was measured by quantifying histone-associated DNA fragments using a Cell Death ELISA Kit. Cells were treated with scrambled or si*EPHA2* for 72 hours before the assay. All 6 cell lines exhibited a statistically significant increase in apoptosis in the cells treated with si*EPHA2* compared with the scrambled controls. Experiments were repeated 3 times, and data are presented as average absorbance unit (AU) ± SEM. (**D**) H2009 and H358 cells were treated with scrambled or si*EPHA2* for 72 hours. Cells were starved for 24 hours and stimulated with 10% serum for 10 minutes before lysis. Shown are representative immunoblots in which phosphorylation levels of signaling molecules were detected using anti-phospho antibodies and EPHA2 expression was detected by an anti-EPHA2 antibody. **P* < 0.05, ***P* < 0.01.

was assessed by weighing the mice daily and by histopathologic examination of vital organs (hearts, kidneys, and livers) at the end of the studies. Mice treated with ALW-II-41-27 did not experience significant weight loss during the course of the study, and no significant histopathologic differences were seen in the heart, liver, or kidney tissue among the various treatment groups (Figure 8B and Supplemental Figure 3). Histological analysis of tumors treated with ALW-II-41-27 showed a significant increase in apoptosis compared with tumors treated with NG-25 or the vehicle alone (Figure 8, C and D), similar to what was seen upon genetic ablation of EPHA2. No significant differences were observed in proliferation or tumor vessel density in ALW-II-41-27–treated tumors compared with NG-25– or vehicle-treated tumors, as measured by PCNA and vWF staining, respectively (Figure 8, E–H). Remarkably, administration of an increased dose of ALW-II-41-27 (30 mg/kg) to tumor-bearing animals resulted in tumor regression (Figure 8I), although some toxicity was observed at this concentration. These data suggest that efforts in further development of EPHA2 inhibitors should focus on increasing efficacy and selectivity while preventing off-target side effects.

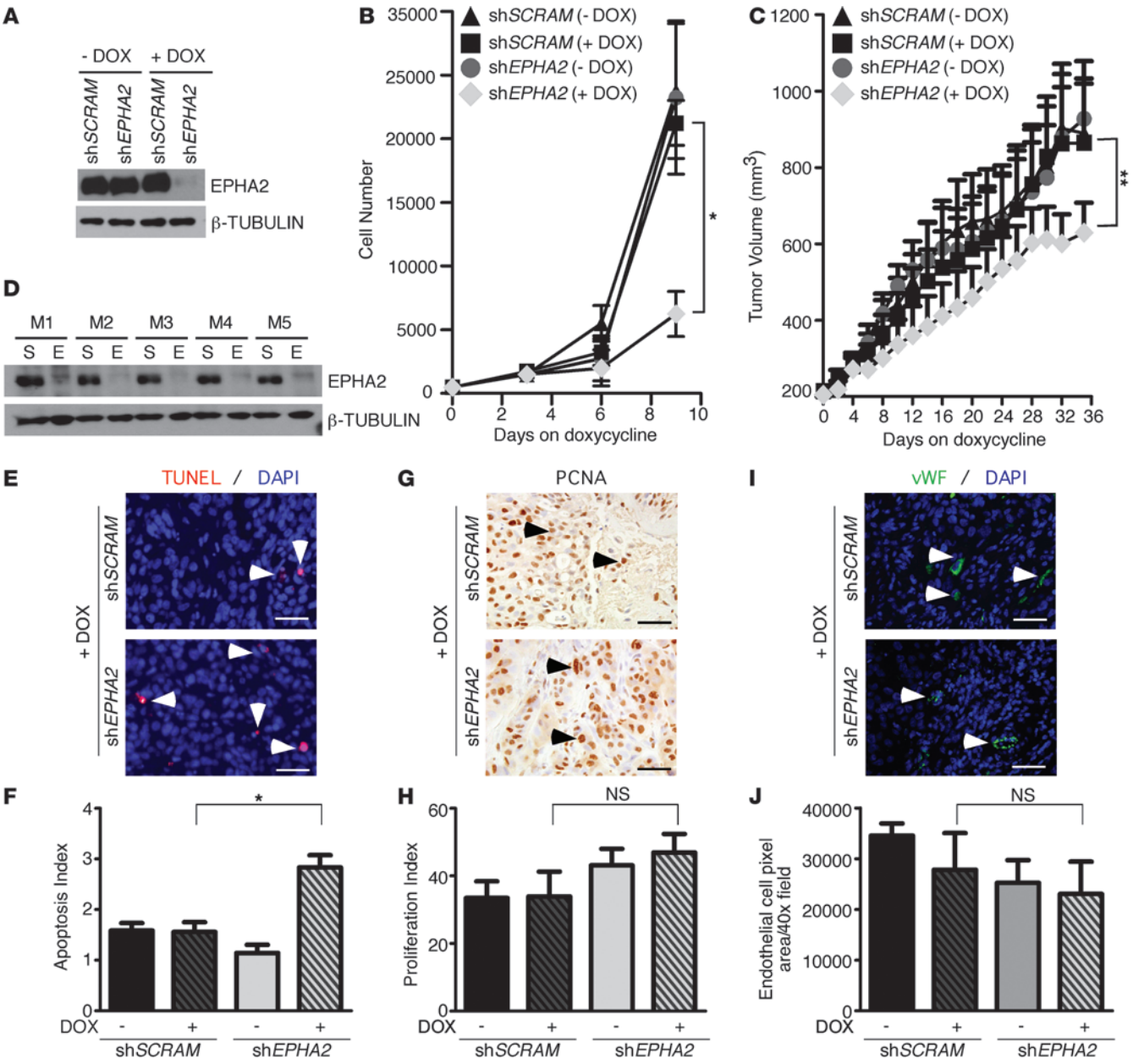

Figure 5

Inducible knockdown of *EPHA2* reduces cell viability in vitro and mitigates tumor growth in vivo. (**A** and **B**) Cells were transduced with lentiviruses carrying either DOX-inducible sh*EPHA2* or scrambled shRNA (sh*SCRAM*). (**A**) Cells were treated with 1 μg/ml DOX for 9 days. Expression of EPHA2 was determined by immunoblotting, and (**B**) cell viability was determined by enumerating live cells over a time course. Shown are average cell numbers ± SEM. (**C**) H358 cells containing DOX-inducible *EPHA2* or scrambled shRNA were injected into the left or right flank in the same nude mouse subcutaneously. Tumors were allowed to grow to 200 mm^3 before administering DOX-containing food pellets or regular mouse chow. Data are presented as the mean tumor volumes ± SEM ($n = 5$ per group). Differences among the 4 treatment groups were analyzed statistically using linear mixed model fit by REML. (**D**) Loss of EPHA2 expression was confirmed in mice fed DOX via immunoblotting of whole tumor lysates harvested at the end of experiment. S, sh*Scrambled*; E, sh*EPHA2*. (**E** and **F**) Apoptosis was determined by TUNEL staining. Apoptosis index is presented as average percentage $TUNEL^+$ nuclei (arrowheads) per total nuclei ± SEM ($n = 5$ tumors per condition). (**G** and **H**) Proliferation was measured by PCNA staining. Proliferation index is presented as the average percentage of $PCNA^+$ nuclei (arrowheads) per total nuclei ± SEM ($n = 5$ tumors per condition). (**I** and **J**) Tumor vasculature was quantified and presented as the mean of vWF^+ pixels (arrowheads) per section ± SEM. ($n = 5$ tumors per condition). Scale bar: 50 μm. $^*P < 0.05$, $^{**}P < 0.01$. n.s., not significant.

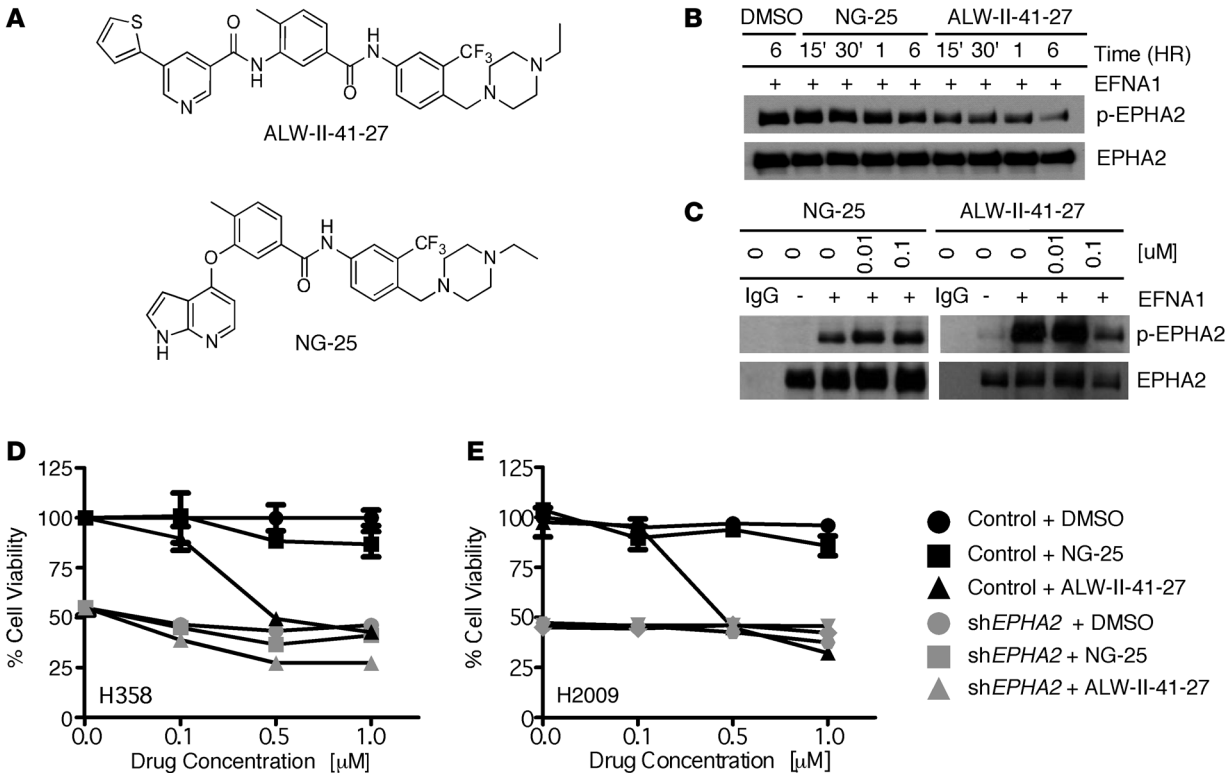

Figure 6

Structure and properties of ALW-II-41-27, a small-molecule kinase inhibitor of EPHA2. (**A**) Chemical structures for ALW-II-41-27 and its structural analog, NG-25. (**B**) H358 cells were treated with 1 μM NG-25 or ALW-II-41-27 over a time course, and cells were stimulated with EPHRIN-A1 ligand (EFNA1, 100 ng/ml) for the last 15 minutes of treatment. EPHA2 was immunoprecipitated, and tyrosine phosphorylation of EPHA2 was determined by Western blot analysis. (**C**) Dose-dependent effect of ALW-II-41-27 on EPHA2 phosphorylation. Cells were treated with inhibitors for 72 hours, including a 15-minute stimulation with EFNA1 at the end of the incubation. Tyrosine phosphorylation of EPHA2 was determined as in **B**. (**D** and **E**) H358 or H2009 cells transduced with lentiviruses containing an empty vector or an *EPHA2*-specific shRNA were treated with ALW-II-41-27, NG-25, or DMSO, and the percentage of viable cells was assessed at 72 hours via the MTT assay. Cells with wild-type levels of *EPHA2* exhibited a marked loss of cell viability in the presence of ALW-II-41-27, while *EPHA2* knockdown cells displayed minimal decrease in cell viability upon ALW-II-41-27 treatment. Data are presented as average percent of cell viability ± SEM.

To investigate the drug-tumor interaction in vivo, tumors from drug-treated animals were analyzed for an interaction between ALW-II-41-27 and EPHA2 in situ using the chemical proteomics platform, KiNativ (23), wherein the extent to which a biotinylated ATP probe covalently binds to the kinase's ATP-binding pocket is measured by mass spectrometry (MS). These studies revealed that the majority of the ATP probe (>95%) was unable to bind EPHA2 in tumors from mice treated with 30 mg/kg ALW-II-41-27, suggesting that the majority of the EPHA2 receptor located on the tumor cells was bound by the EPHA2 inhibitor in vivo. In contrast, other EPH family receptors, such as EPHB2 and EPHB3, retained the ATP probes, leaving 52% and 45% of the ATP probe unbound, thus confirming specificity of ALW-II-41-27 for EPHA2 above other EPH family RTKs. Additionally, ALW-II-41-27 had a low affinity in vivo for other kinases, such as EGFR, ERK, HER2, and PIK3CA (Figure 8J and Supplemental Table 2). ALW-II-41-27 can potently bind to several intracellular kinases, including ABL, p38, ZAK, and several SRC-family kinases, but these targets were also engaged by the structural analog, NG-25, which did not inhibit tumor growth in vivo (Supplemental Table 2). Collectively, EphA2 is the most dramatically distinct target engaged by ALW-II-41-27 as compared with NG-25, which is consistent with EPHA2 being a functionally important target of ALW-II-41-27 in NSCLC.

Discussion

Genome-wide analyses identified overexpression of the RTK EPHA2 in NSCLCs. While previous studies have provided correlative data linking high EPHA2 levels to poor clinical outcome in human lung cancer populations (10–12), the biology underlying these observations and translational potential of these correlations remain underexplored. Here, we show the first functional evidence that EPHA2 promotes tumor growth and survival in a large panel of NSCLC lines, in human tumor xenografts, and in a transgenic mouse model of aggressive *Kras*-mutant lung cancer. We show that S6K1-dependent BAD phosphorylation is one of the key signaling events mediating the EPHA2-regulated cell survival pathway. We also identified an EPHA2 kinase inhibitor, ALW-II-41-27, that suppresses cell viability in vitro and induces tumor regression of human NSCLC xenografts in vivo, demonstrating the translational potential of targeting EPHA2 in lung cancer.

To assess the subtypes of lung cancer most sensitive to EPHA2 inhibition, we analyzed a panel of 14 NSCLC cell lines carrying the 6 most common mutations present in patients with lung cancer.

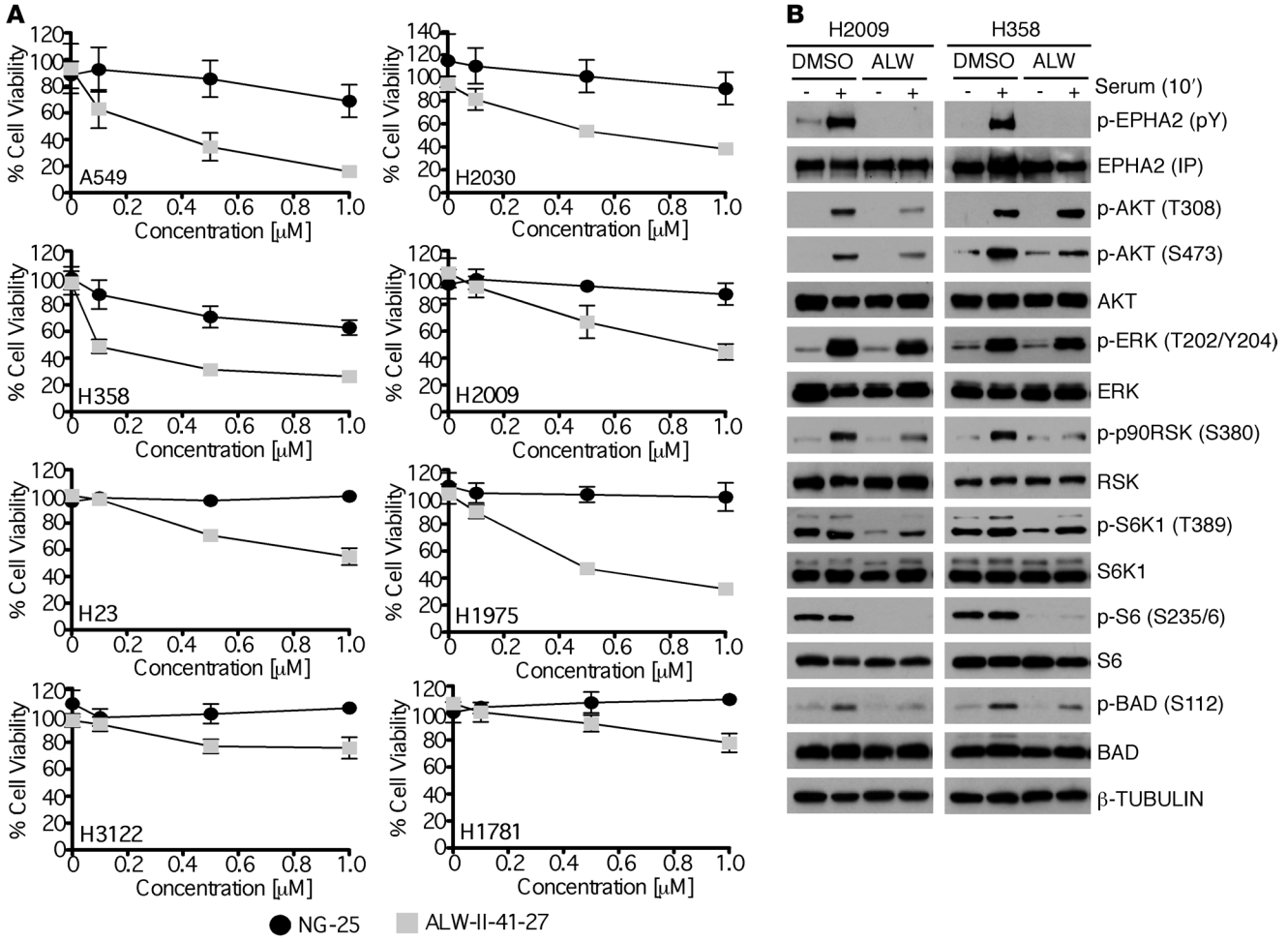

Figure 7

ALW-II-41-27 treatment leads to decreased cell viability in NSCLC cell lines. (**A**) NSCLC cell lines were treated with ALW-II-41-27, NG-25, or DMSO for 72 hours, and cell viability was assessed by the MTT assay. Shown are percentages of cell viability ± SEM in drug treatment groups relative to a DMSO control group. (**B**) H2009 and H358 cells were treated with 1 μM ALW-II-41-27 or DMSO for 6 hours. Cells were starved 24 hours and stimulated with 10% serum-containing media 10 minutes before lysis. EPHA2 was pulled down in immunoprecipitation and immunoblotted for pY99 and pY20 (represented here as p-EPHA2 [pY]). Phosphorylation of other signaling molecules was determined by Western blot analyses using anti-phospho or anti-total protein antibodies as indicated. Shown are blots representative of 2 to 3 independent experiments for each signaling molecule.

Knockdown of EPHA2 expression inhibits tumor cell viability in the majority of cell lines tested, most dramatically affecting cell lines bearing *KRAS* mutations. However, sensitivity to EPHA2 inhibition does not correlate strictly with *KRAS* mutation status. Rather, EPHA2 receptor phosphorylation levels appeared to be important in determining whether a given tumor cell line is sensitive to *EPHA2* knockdown (Supplemental Figure 1, B and C). Therefore, although targeting EPHA2 is effective in *KRAS* mutant NSCLC, it is not exclusive to *KRAS* mutant NSCLC. The utility of targeting EPHA2 in *KRAS* mutant NSCLC is further supported by our in vivo data, which show that either genetic or pharmacologic inhibition of EPHA2 in *KRAS* mutant lung tumors promotes apoptosis and inhibits tumor growth. Because there is currently no effective targeted therapy for treating *KRAS* mutant lung cancer, EPHA2 provides a promising alternative target for this subtype of lung cancer.

Previous studies have shown that RAS/MAPK signaling induces EPHA2 expression and ligand-stimulated EPHA2 forward signaling in turn attenuates growth factor–induced RAS activity, forming a negative feedback loop in normal epithelial cells (24). An escape from the negative effects of this interaction has been suggested to be important in the development of cancer (24). Indeed, our lab and others demonstrated that ligand-independent EPHA2 signaling and cross-talk with other oncogenic pathways serve to promote tumor cell proliferation and motility in breast cancer and glioma (8, 9, 25). Consistent with these findings, the tumor promotion role of EPHA2 in lung cancer appears to be ligand-independent, as exogenous EPHRIN-A1 stimulation inhibits tumor cell proliferation (26). In this study, we showed that genetic and pharmacologic inhibition of EPHA2 induces apoptosis in lung cancer. Interestingly, loss of EPHA2 does not appear to significantly affect the activities of ERK but rather inhibits cell survival by modulating mitochondrial apoptosis through p90-RSK/S6K1-induced inactivation of the proapoptotic protein BAD. These studies suggest that EPHA2 could serve as an attractive target for therapeutic intervention in lung cancer.

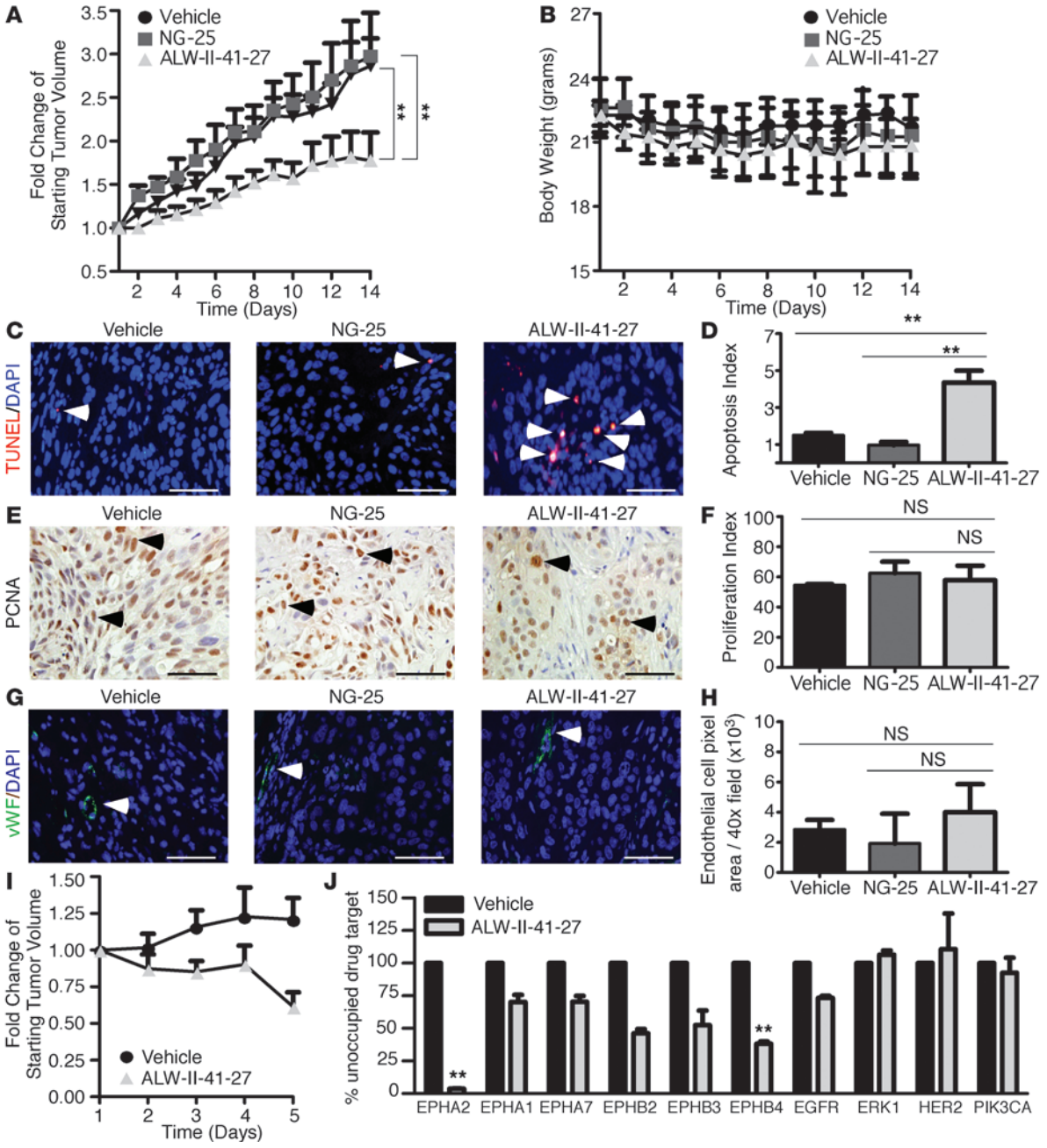

Figure 8

ALW-II-41-27 inhibits NSCLC tumor growth in vivo. (**A**) 15×10^6 H358 cells were injected subcutaneously into the dorsal flanks of nude mice. Tumors were allowed to grow to 200 mm^3 before administration of 15 mg/kg NG-25, ALW-II-41-27, or vehicle alone via intraperitoneal injection twice daily. Tumor size was measured every day with a digital caliper, and tumor volumes were calculated. Data are presented as the fold change of starting tumor volumes ± SEM (n = 5 per condition). (**B**) No statistical difference in body weight was detected among any of the treatment groups during the course of treatment. Data are presented as average body weight ± SEM. (**C** and **D**) Tumors were harvested at the termination of the study, and apoptosis was assessed via TUNEL staining. An apoptosis index of the tumor sections is presented as TUNEL-positive nuclei (arrowheads) per total nuclei ± SEM. (**E** and **F**) Proliferation in tumors treated with NG-25, ALW-II-41-27, or vehicle alone was quantified as the total number of PCNA-positive nuclei (arrowheads) relative to the total nuclei ± SEM. (**G** and **H**) No change in tumor vessel density (arrowheads) was detected by vWF staining. Data are presented as average endothelial cell pixel area ± SEM. (**I**) Tumor regression was observed when H358 xenografts (as in **A**) were treated with an increased dose of ALW-II-41-27 (30 mg/kg) over 5 days (n = 5 per condition). Data are presented as percent of change in tumor volume ± SEM. (**J**) Drug-target interaction in xenograft tumors in situ was determined by the chemical proteomics platform KiNativ (see Methods). Shown are percentages of drug targets unoccupied by ALW-II-41-27 relative to vehicle control. Data are presented as percent of unoccupied drug target ± SEM. $^{**}P < 0.01$, Student's t test (n = 5 tumors per group). Scale bar: 50 μm.

The effect of systemic loss of *EPHA2* through gene targeting on tumor growth may be due to loss of EPHA2 in the tumor epithelia and within the tumor microenvironment. In support of an epithelial-autonomous role for EPHA2 in NSCLCs, inducible shRNA-mediated *EPHA2* knockdown in NSCLC xenografts showed reduced tumor progression but to a lesser extent than systemic genetic knockout (Figures 1 and 2) or systemic pharmacologic inhibition (Figure 8). These studies are consistent with previous reports that EPHA2 expressed in endothelial cells promotes tumor angiogenesis (16, 27, 28). Because EPHA2 is important in both tumor cells and their microenvironment, inhibition of EPHA2 may provide a dual benefit toward eradicating cancers.

This study identified a type II kinase inhibitor, ALW-II-41-27, that inhibits EPHA2 kinase activity and causes NSCLC tumor regression in vivo. As is true for most kinase-targeted drugs, ALW-II-41-27 also inhibits other targets. Four lines of evidence indicate that EPHA2 is a functionally important target of ALW-II-41-27. First, NG-25, a structural analog with a similar target spectrum as ALW-II-41-27, but which does not inhibit EPHA2 RTK, displayed limited effects on cell viability in vitro and tumor growth in vivo. Second, signaling studies in cells treated with ALW-II-41-27 recapitulated what was observed in *EPHA2* knockdown cells, suggesting that EPHA2 is a major target of the compound. Third, depletion of *EPHA2* by RNAi rendered NSCLC cells much less sensitive to the effects of ALW-II-41-27, relative to the undepleted controls, consistent with EPHA2 being a functionally important target of the compound. Finally, in situ drug-tumor interaction studies using "KiNativ" MS demonstrated the selectivity of ALW-II-41-27 for EPHA2 within the EPH receptor family as well as among other kinases.

To assess whether EPHA2 inhibition has the potential to affect patient outcomes, we compared the effectiveness of ALW-II-41-27 with erlotinib in 4 cell lines carrying mutant *KRAS* (H2009 and H358), *EGFR* (PC-9), or *MEK-1* (H1437). As expected, erlotinib is only efficacious in PC-9 cells expressing mutant *EGFR*, whereas ALW-II-41-27 also inhibits cell viability in 2 cell lines carrying *KRAS* mutations (Supplemental Figure 4). In PC-9 cells, erlotinib is approximately 5-fold more potent than ALW-II-41-27. However, the approximately 500 nM antiproliferative IC_{50} of ALW-II-41-27 represents a good starting point for further medicinal chemistry efforts to yield a compound with suitable properties for clinical evaluation. In addition, although targeting EPHA2 does not exclusively affect mutant *KRAS* tumors, EPHA2 inhibitors provide promise for treating *KRAS* mutant lung cancer, as there is currently no effective targeted therapy for treating this subtype of lung cancer.

In summary, we have provided genetic, functional, mechanistic, and pharmacologic evidence that EPHA2 signaling promotes the progression and survival of NSCLC. Furthermore, this study identified a new category of EPHA2 kinase inhibitors that hold promise for therapeutics in NSCLCs, even for those driven by activating *KRAS* mutations.

Methods

Tumor studies in mutant Kras knockin mice

$Kras^{LA2}$ mice harboring the $Kras^{G12D}$ mutation (17) were provided by Ambra Pozzi (Vanderbilt University). $Kras^{LA2}$ mice were crossed with *EphA2* heterozygous mice (29) on the C57BL/6 background to generate $Kras^{G12D}EphA2^{+/+}$ and $Kras^{G12D}EphA2^{-/-}$ mice. Age-matched $Kras^{G12D}EphA2^{+/+}$ and $Kras^{G12D}EphA2^{-/-}$ littermates were sacrificed at 3 different time points: 15, 20, and 25 weeks of age. Genotypes were confirmed for each animal in the study 2 independent times by analyzing genomic DNA of both tail and ear tissues, respectively. *EphA2* primers were 5′-GGGTGCCAAAGTAGAACTGCG-3′ (forward), 5′-GACAGAATAAAACGCACGGGTG-3′ (Neo), and 5′-TTCAGCCAAGCCTATGTAGAAAGC-3′ (reverse) (29). *Kras* primers were 5′-TGCACAGCTTAGTGAGACCC-3′ (common forward), 5′-GACTGCTCTCTTTCACCTCC-3′ (wild-type reverse), and 5′-GGAGCAAAGCTGCTATTGGC-3′ (mutant reverse). Lungs removed for analysis were first perfused with 1× PBS followed by 10% buffered formalin (Fisher). Lungs were weighed after 24 hours of fixation in formalin. Lung tumor surface area was calculated by measuring a length (l) and width (w) of each surface tumor nodule and using the area calculation $([l + w]/4)^2 \times \pi$.

MRI

Mice were anesthetized via inhalation of 2%:98% isoflurane/oxygen. Animals were secured in a prone position in a 38-mm inner diameter radiofrequency coil and placed in a Varian 7T horizontal bore imaging system (Varian Inc.) for data collection. For each animal, multislice scout images were collected in all 3 imaging planes (axial, sagittal, and coronal) for subsequent localization of the lungs, using a gradient echo sequence with repetition time = 75 ms, echo time = 4 ms, slice thickness = 2 mm, flip angle = 30°, and an average of 4 acquisitions. Additional parameters include field of view = 32 mm × 32 mm and data matrix = 128 × 128. Following localization of the lungs, a respiratory-triggered T2-weighted fast-spin echo imaging sequence was used to acquire image slices in the axial plane, with field of view = 25.6 mm × 25.6 mm, slice thickness = 1 mm, repetition time = 2 seconds, effective echo time = 36 ms, data matrix = 256 × 256, and an average of 16 acquisitions, with a total acquisition time of approximately 25 minutes per animal. Following image acquisition, lung tumor volume measurements were performed using Matlab 2012a (The MathWorks Inc.). A region of interest encompassing the entire lung was manually drawn for each slice, and a signal intensity threshold of 25 times the noise level (defined as the standard deviation of signal intensities in a region of the image background) was used to segment voxels within that region of interest as positive for tumor. Total lung tumor volume was then calculated as the sum of the number of voxels within the segmented tumor region multiplied by the volume of each voxel.

Immunohistochemistry

Whole lungs and tumors were harvested at the indicated time points and fixed in 10% buffered formalin (Fisher). Immunohistochemical staining for EPHA2 and PCNA was performed as described previously (27). A proliferation index was calculated as the average percentage of $PCNA^+$ nuclei relative to total nuclei (4 fields of at least 5 tumors per genotype or treatment condition were assessed). Apoptosis assays were performed using the Apoptag Red In Situ Apoptosis Detection Kit per the manufacturer's protocol (Millipore). An apoptosis index was measured as the percentage of $TUNEL^+$ nuclei relative to total nuclei (4 fields of at least 5 independent tumors per genotype or treatment condition were assessed). Immunofluorescence staining for vWF was performed as described previously (16). Tumor vessel density was determined by assessing the vWF^+ vessels (pixels) in 4 fields per sample of at least 5 independent tumors per genotype or treatment condition. Antibodies against the following proteins were used: EPHA2 (Invitrogen; 347400), PCNA (BD Biosciences), vWF (Dako Cytomation), biotin goat anti-rabbit (BD Pharmingen), and anti-rabbit Cy3 (Jackson ImmunoResearch). Additionally, retrievagen A (pH 6.0) (BD Pharmingen, 550524), streptavidin peroxidase reagents (BD Pharmingen, 51-75477E), and the liquid 3,3′-diaminobenzidine tetrahydrochloride substrate kit (Zymed Laboratories) were used. Cytoseal XYL (Richard Allan Scientific) or ProLong Gold antifade reagent with DAPI (Life Technologies) were used to mount slides.

Cell culture

The human NSCLC lines were provided by David Carbone, William Pao, and Pierre Massion (Vanderbilt University). 293T cells were purchased from the ATCC. All NSCLC cells were maintained in RPMI 1640 medium (Corning/Cellgro) supplemented with L-glutamine (2 mM), penicillin (100 U/ml), streptomycin (100 μg/ml), and 10% fetal bovine serum (Thermo Scientific, HyClone Laboratories Inc.). 293T cells were maintained in DMEM (Corning/Cellgro) supplemented with L-glutamine (2 mM), penicillin (100 U/ml), streptomycin (100 μg/ml), and 10% fetal bovine serum (Thermo Scientific, HyClone Laboratories Inc.). Authenticity of the cells was verified by DNA profiling, flow cytometry, or immunohistochemistry. Cells were grown in a humidified incubator with 5% CO_2 at 37°C. Stable cell lines generated with the pLKO.1 and pTRIPZ vectors were maintained in 1 to 2 μg/ml of puromycin containing complete media. For cells transduced with the pTRIPZ vector, production of shRNA was initiated with addition of 1 μg/ml DOX (Sigma-Aldrich) to the media, which was refreshed every 3 days. *EPHA2* ON-TARGETplus Human SMARTpool siRNA (L-003116-00-0005) and ON-TARGETplus Non-Targeting pool siRNA (D-001810-10-05) (Dharmacon/Thermo Scientific) were used at a concentration of 12.5 nM in conjunction with Lipofectamine RNAiMAX transfection reagent (Invitrogen) according to the manufacturer's protocol. Stable *EPHA2* knockdown cells lines were created by lentiviral transduction of a pLKO.1 vector containing *EPHA2*-specific shRNA constructs (sh*EPHA2* no. 1 mature sense 5′-CGGACAGACATATAGGATATT-3′ or sh*EPHA2* no. 2 mature sense 5′-GCGTATCTTCATTGAGCTCAA-3′). Plasmids were obtained from Open Biosystems. Inducible sh*EPHA2* (5′-AAGGAGACTTTCAACCTCT-3′) and scrambled control plasmid constructs (pTRIPZ) from Open Biosystems were also used.

Cell viability assays

MTT assay. Cells were seeded in 100 μl media in 96-well plates at a density of 4,000 cells per well. On the final day of the assay, 20 μl of 5 mg/ml of thiazolyl blue tetrazolium bromide (MTT) (Sigma-Aldrich) in PBS was added and incubated at 37°C for 2 hours. The MTT solution was aspirated, and an isopropanol solution with 4 mM HCl and 0.1% Nonidet P-40 was added and incubated at room temperature for 10 minutes. The absorbance was read on a spectrophotometer (BioTEK) at 590 nm. All experimental points were set up with at least 6 replicates and were performed at least 2 independent times. Cell viability was presented as a percentage of cells transduced with an empty vector, transfected with scrambled siRNA, or treated with a vehicle alone.

Cell death ELISA. Cells were seeded along with RNAiMAX transfection reagent and appropriate siRNAs (12.5 nM final concentration). At 72 hours after transfection, cells were washed once with PBS and lysed as per the manufacturer's instructions (Cell Death Detection ELISA PLUS kit, Roche). Detection of histone-associated DNA fragments in the lysate was measured using biotin labeled anti-histone and peroxidase-conjugated anti-DNA antibodies. Signal was detected upon the addition of the peroxidase substrate ABTS, and the absorbance was measured at 405 nm wavelength.

TUNEL assay. TUNEL was used to assess apoptosis. Cells were seeded on 8-well chamber slides (Lab-Tek), and the Apoptag Red In Situ Apoptosis Detection Kit (Millipore) was used according the manufacturer's instructions. Four representative images were taken of the TUNEL staining, with corresponding DAPI staining, and the number of TUNEL-positive nuclei relative to total nuclei per image was counted and calculated. Data are representative of at least 2 independent experiments.

Antibodies and immunoblotting

Antibodies against the following proteins were used: EPHA2 (D7, mouse monoclonal, 1:1,000, Millipore); phospho-tyrosine pY20 and pY99 (mouse monoclonal, 1:1,000, Santa Cruz Biotechnology); β-tubulin (mouse monoclonal, 1:2,000, Sigma-Aldrich); p-AKT(S473 and T308), AKT, p-ERK(T202/Y204), ERK, p-P90RSK(S380), RSK, p-S6K1(T389), S6K1, p-S6(S235/6), S6, p-BAD(S112), BAD (all rabbit monoclonal, 1:1,000, Cell Signaling Technology); cleaved caspase-3, caspase-3, and cleaved PARP (all rabbit, 1:500, Cell Signaling Technology). HRP-conjugated anti-mouse and anti-rabbit antibodies were used, respectively. For immunoblotting, cells were washed with 1x PBS and lysed on ice with RIPA buffer supplemented with a protease inhibitor cocktail (P8340) (Sigma-Aldrich) and phosphatase inhibitors (Roche Diagnostics). Lysates were subjected to SDS/PAGE followed by blotting with the indicated antibodies. Signal detection was achieved using Clarity Western ECL substrate (Bio-Rad).

Tumor xenograft

H358 cells (15×10^6 cells) containing a DOX-inducible scrambled or *EPHA2* knockdown sequence (pTRIPZ) were injected with Matrigel into opposing hind flanks of 6-week-old athymic nude mice (Foxn1^{nu}) (Harlan). When tumors reached approximately 150–250 mm^3, animals were randomized to receive either a DOX-containing diet (TD.00426, Harlan) or a standard mouse diet. Tumors were measured every 2 days using digital calipers. Volumes were calculated using the following formula: volume = length × width^2 × 0.52.

For inhibitor studies, 15×10^6 H358 cells were injected with Matrigel into the hind flanks of 6-week-old athymic nude mice (Foxn1^{nu}) (Harlan). Once tumors reached 150–250 mm^3, animals received either 15 mg/kg (Figure 8A) or 30 mg/kg (Figure 8I) of ALW-II-41-27 or NG-25 in 10% 1-methyl-2-pyrrolidinone and 90% PEG 300 or the vehicle alone. Mice were treated 2 times daily via intraperitoneal injection, and tumors were measured daily with digital calipers. Volumes were calculated using the following formula: volume = length × width^2 × 0.52.

Kinase inhibitor screen and analysis of drug-target interaction in vivo

ALW-II-41-27 and NG-25 were synthesized in the lab of Nathanael Gray. The inhibitors were dissolved in DMSO for all in vitro studies. In situ drug-target interaction in tumor xenografts was analyzed by a chemical proteomics platform, KiNativ, at ActivX Inc., as described previously (23, 30). Tumor lysate was incubated with ATP-biotin labeled probes to assess which kinases received protection from the drug binding via MS analysis. Based on the resulting data set, parent ions corresponding to each kinase were selected for targeting and were assembled into a time-segmented target list using the instrument control software XCalibur 2.2. All MS data were analyzed using custom software that was designed to extract and normalize signals from relevant probe-labeled peptides. Signals were normalized based on the average signal ratios of major parent ions throughout the run. For signal extraction/quantitation, typically up to 4 ions were selected based on their presence, intensity, and correlation to the reference MS/MS spectrum. The resulting chromatographic peaks from each run were then integrated, and the integrated peak areas were used to determine percent inhibition values relative to control runs. Enzymatic IC_{50} data in Supplemental Table 2 were generated by in vitro kinase assays that were conducted at Life Technologies using the SelectScreen Kinase Profiling Service.

Statistics

For animal studies, linear mixed models were used to estimate the effects of treatment and genotype on tumor volume change over time and to account for potential correlation of within subject measurement. Possible values of the variable are from round 1 or round 2 of the duplicated experiment. In addition to estimated effect sizes and information criteria, *P* values for fixed-effects terms were calculated for a better understanding

of findings by performing a likelihood ratio test for each term and model. These analyses were performed using R 2.15.1. For other studies, 2-tailed Student's *t* test was used for comparisons between 2 groups, and ANOVA or Kruskal-Wallis tests were used for analysis with multiple comparisons. All tests of statistical significance were 2 sided, and *P* values of less than 0.05 were considered to be statistically significant.

Study approval

All animal experiments were conducted under guidelines approved by the AAALAC and Vanderbilt University Institutional Animal Care and Use Committee.

Acknowledgments

We would like to thank David Carbone, William Pao, and Pierre Massion for advice and helpful discussion. We would also like to acknowledge Matthew Patricelli and Tyzoon Nomanbhoy (ActivX Biosciences) for analysis of drug-target interaction in situ in xenograft tumors using the proteomics platform KiNativ. This work was supported by Department of Veterans Affairs through a VA Merit Award (to J. Chen), NIH grants R01 CA95004 (to J. Chen) and R01 CA173469 (to N. Gray), NIH grant F-31 CA167878 (to K. Amato), pilot projects from the SPORE program P50CA090949 and VICC thoracic program (to J. Chen), and the Vanderbilt International Scholar Program (to H. Chen). This work was also supported in part by the NCI Cancer Center Support Grant P30 CA068485, utilizing the Translational Pathology, Flow Cytometry, and Small Animal Imaging Shared Resources.

Received for publication January 9, 2014, and accepted in revised form February 20, 2014.

Address correspondence to: Jin Chen, Professor of Medicine and Cancer Biology, T-3207E, Medical Center North, Vanderbilt University School of Medicine, 1161 21st Avenue South, Nashville, Tennessee 37232, USA. Phone: 615.343.3819; Fax: 615.343.8648; E-mail: jin.chen@vanderbilt.edu.

1. Beer DG, et al. Gene-expression profiles predict survival of patients with lung adenocarcinoma. *Nat Med*. 2002;8(8):816–824.
2. Rohrbeck A, et al. Gene expression profiling for molecular distinction and characterization of laser captured primary lung cancers. *J Transl Med*. 2008;6:69.
3. Zhu CQ, et al. Prognostic and predictive gene signature for adjuvant chemotherapy in resected non-small-cell lung cancer. *J Clin Oncol*. 2010; 28(29):4417–4424.
4. Ding L, et al. Somatic mutations affect key pathways in lung adenocarcinoma. *Nature*. 2008;455(7216):1069–1075.
5. Kullander K, Klein R. Mechanisms and functions of Eph and ephrin signaling. *Nat Rev Mol Cell Biol*. 2002;3(7):475.
6. Pasquale EB. Developmental Cell Biology: Eph receptor signalling casts a wide net on cell behaviour. *Nat Rev Mol Cell Biol*. 2005; 6(6):462–475.
7. Pasquale EB. Eph-ephrin bidirectional signaling in physiology and disease. *Cell*. 2008;133(1):38–52.
8. Larsen AB, Pedersen MW, Stockhausen MT, Grandal MV, van Deurs B, Poulsen HS. Activation of the EGFR gene target EphA2 inhibits epidermal growth factor-induced cancer cell motility. *Mol Cancer Res*. 2007;5(3):283–293.
9. Brantley-Sieders DM, et al. The receptor tyrosine kinase EphA2 promotes mammary adenocarcinoma tumorigenesis and metastatic progression in mice by amplifying ErbB2 signaling. *J Clin Invest*. 2008;118(1):64–78.
10. Brannan JM, et al. Expression of the receptor tyrosine kinase EphA2 is increased in smokers and predicts poor survival in non-small cell lung cancer. *Clin Cancer Res*. 2009;15(13):4423–4430.
11. Faoro L, et al. EphA2 mutation in lung squamous cell carcinoma promotes increased cell survival, cell invasion, focal adhesions, and mTOR activation. *J Biol Chem*. 2010;285(24):18575–18585.
12. Kinch MS, Moore MB, Harpole DHJ. Predictive value of the EphA2 receptor tyrosine kinase in lung cancer recurrence and survival. *Clin Cancer Res*. 2003;9(2):613–618.
13. Zhuang G, et al. Elevation of receptor tyrosine kinase EphA2 mediates resistance to trastuzumab therapy. *Cancer Res*. 2010;70(1):299–308.
14. Brantley-Sieders DM, et al. Eph/ephrin profiling in human breast cancer reveals significant associations between expression level and clinical outcome. *PLoS One*. 2011;6(9):e24426.
15. Fang WB, Brantley-Sieders DM, Parker MA, Reith AD, Chen J. A kinase-dependent role for EphA2 receptor in promoting tumor growth and metastasis. *Oncogene*. 2005;24(53):7859–7868.
16. Brantley-Sieders DM, Fang WB, Hicks D, Koyama T, Shyr Y, Chen J. Impaired tumor microenvironment in EphA2-deficient mice inhibits tumor angiogenesis and metastatic progression. *FASEB J*. 2005;19(13):1884–1886.
17. Johnson L, et al. Somatic activation of the K-ras oncogene causes early onset lung cancer in mice. *Nature*. 2001;410(6832):1111–1116.
18. Zha J, Harada H, Yang E, Jockel J, Korsmeyer SJ. Serine phosphorylation of death agonist BAD in response to survival factor results in binding to 14-3-3 not BCL-X(L). *Cell*. 1996;87(4):619–628.
19. Harada H, Andersen JS, Mann M, Terada N, Korsmeyer SJ. p70S6 kinase signals cell survival as well as growth, inactivating the pro-apoptotic molecule BAD. *Proc Natl Acad Sci U S A*. 2001; 98(17):9666–9670.
20. Choi Y, et al. Discovery and structural analysis of Eph receptor tyrosine kinase inhibitors. *Bioorg Med Chem Lett*. 2009;19(15):4467–4470.
21. Liu Y, Gray NS. Rational design of inhibitors that bind to inactive kinase conformations. *Nat Chem Biol*. 2006;2(7):358–364.
22. Dzamko N, et al. The IkappaB kinase family phosphorylates the Parkinson's disease kinase LRRK2 at Ser935 and Ser910 during Toll-like receptor signaling. *PLoS One*. 2012;7(6):e39132.
23. Patricelli MP, et al. In situ kinase profiling reveals functionally relevant properties of native kinases. *Chem Biol*. 2011;18(6):699–710.
24. Macrae M, et al. A conditional feedback loop regulates Ras activity through EphA2. *Cancer Cell*. 2005;8(2):111–118.
25. Miao H, et al. EphA2 mediates ligand-dependent inhibition and ligand-independent promotion of cell migration and invasion via a reciprocal regulatory loop with Akt. *Cancer Cell*. 2009;16(1):9–20.
26. Brannan JM, et al. EphA2 in the early pathogenesis and progression of non-small cell lung cancer. *Cancer Prev Res*. 2009;2(12):1039–1049.
27. Brantley DM, et al. Soluble EphA receptors inhibit tumor angiogenesis and progression in vivo. *Oncogene*. 2002;21(46):7011–7026.
28. Chen J. Regulation of tumor initiation and metastatic progression by Eph receptor tyrosine kinases. *Adv Cancer Res*. 2012;114:1–20.
29. Brantley-Sieders D, Caughron J, Hicks D, Pozzi A, Ruiz JC, Chen J. EphA2 receptor tyrosine kinase regulates endothelial cell migration and assembly through phosphoinositide 3-kinase-mediated Rac1 GTPase activation. *J Cell Sci*. 2004; 117(pt 10):2037–2049.
30. Patricelli MP, et al. Functional interrogation of the kinome using nucleotide acyl phosphates. *Biochemistry*. 2007;46(2):350–358.